SRTTU

JCARME
ISSN: 2228-7922
Journal of Computational and Applied Research in Mechanical Engineering
Vol. 9, No. 1, pp. 31-43
jcarme.sru.ac.ir

Numerical investigation on the effects of six control rods arranged in equilateral triangular configurations on the fluid flow and forced convection heat transfer from a circular cylinder

S. Harimi[a] and Azam Marjani[b,c*]

[a]Department of Chemistry, Arak Branch, Islamic Azad University, Arak, Iran
[b]Department for Management of Science and Technology Development, Ton Duc Thang University, Ho Chi Minh City, Vietnam
[c]Faculty of Applied Sciences, Ton Duc Thang University, Ho Chi Minh City, Vietnam

Article info:
Received: 22/06/2017
Accepted: 21/02/2019
Online: 25/02/2019

Keywords:
Control rod,
Equilateral triangular,
Vortex street,
Heat transfer,
Overset grid method.

Abstract
The present work deals with heat transfer characteristics as well as fluid flow patterns in a laminar flow regime for a circular cylinder with six control rods arranged in equilateral triangular geometries. The computations are carried out by a finite volume approach using the overset grid method. The unsteady flow at Re= 200, Pr= 0.7 and 7.0 is examined. Effect of the control rods on the suppression of the fluid forces applied on a main cylinder is investigated by numerical solution of the Navier-Stokes equations. Based on the results obtained, the arrangement employed in this study indicates the significant performance in reducing the oscillatory force coefficients of the primary cylinder. Except for some gap ratios, it is indicated that both drag and lift coefficients are much lower than that for a single cylinder. Moreover, forced convection heat transfer is calculated using local and mean Nusselt numbers at the surface of the cylinders. The instantaneous streamlines, the vortices and isothermal contours are presented in order to analyze the temperature field and flow field around the cylinders.

Nomenclature

a	Thermal diffusivity
C_D	Drag coefficient
T_w	Temperature of the cylinder wall
C_L	Lift coefficient
T_∞	Temperature of the free stream
C_{DF}	Friction drag coefficient
U	Flow velocity vector
C_{Dp}	Pressure drag coefficient
U_x, U_y	Components in Cartesian coordinates
C_{LF}	Friction lift coefficient
u_∞	Velocity of the free stream
C_{LP}	Pressure lift coefficient
x*, y*	Cartesian coordinates
D	Diameter of the primary cylinder

Greek Symbols

d	Diameter of rod
α	Flow incidence angle

*Corresponding author
Email address: azam.marjani@tdtu.edu.vn

Nu	Nusselt number
ɵ	Dimensionless temperature
P^*	Pressure
N	Kinematic viscosity
Pr	Prandtl number ($=v/a$)
ρ	Density of the fluid
Re	Reynolds number
Φ	Angular displacement
St	Strouhal number
T	Temperature
t^*	Time

1. Introduction

The prediction of fluid flow and heat transfer properties around multiple cylinders is crucial in the design and optimization of ocean structures like offshore platforms and pipelines, and many studies have been done in this area [1-3]. It has been recognized that the interaction between these objects is dependent on a number of items, like the dimension of the floating objects and the gap between them. The size gradient in a multi-cylindrical structure is an important parameter, as it can create uneven distributions [4]. In such structures, the dynamic interaction between the shed vortices and the shear layers in the wake behind cylinders lead to the complexity of the wake structure and flow patterns.

On the other hand, the alternate vortex shedding in the wake behind a cylinder can cause large-scale oscillations resulting in fatigue damage. Using small diameter cylinders is effective in the decrease of the various forces applied to the main cylinder. Also, the vortex shedding can modify the pressure fields on the cylinder's surface resulting in an increase of heat transfer. In fact, the interaction among the wakes behind the cylinders and the thermal boundary layer affects the increase in heat transfer. Therefore, the study on cylindrical-shape bodies with various sizes in order to evaluate and control the vortex shedding is critical. A number studies have been reported to analyze the influence of the small rods on the flow field surrounding the large cylinder and on vortex induced vibration (VIV) suppression. Igarashi [5] studied experimentally the variation of the drag coefficient of a square prism attached by a small cylinder. The Reynolds number was fixed at 3.2×10^4. He reported that in the range of $0.1 \leq L/d \leq 2.0$, the drag force of the prism is decreased by about 50% at $G > G_c$ and 70% at $G \leq G_c$. Dalton et al. [6] indicated that the existence of a small rod at the proximity of the main cylinder can be effective at controlling VIV by the elimination of vortex shedding from the primary cylinder for $\mathrm{Re} \leq 3000$. It was also found that the suppression of vortex shedding was sensitive to both the position of the small rod and the angle of attack of the flow.

Decreasing of force coefficients of an isolated cylinder and of two cylinders in different configurations by using tripping rods was examined by Alam et al. [7]. The diameter of tripping rods used was 4×10^{-3}, 5×10^{-3} and 6×10^{-3} m, and the Reynolds number was adjusted at 5.5×10^4. In their study, the position of optimum angular of small rods for decreasing force coefficients of a single cylinder was identified. Moreover, by varying the angular position of small rods, three various flow regimes on the isolated cylinder were revealed. Huang et al. [8] investigated the flow, past rows of various diameters cylinder, at Reynolds numbers below 150. They observed that Karman vortices were not formed for the case of the in-line arrangement of two rows of cylinders of various diameters and two in-line cylinders behaved like one slender body. Carmo et al. [9] performed two- and three-dimensional direct numerical simulations of the flow around two circular cylinders in tandem configurations. The Reynolds number was set 150 for the 2D simulations and 300 for the 3D simulations, and the center to center distance was varied from 1.5 to 8 diameters. It was observed that in comparison with an isolated cylinder, there were significant changes in the dynamic behavior of the cylinders. They attributed these changes to be the oscillatory flow in the gap between the cylinders. By carrying out numerical simulations, Lu et al. [10] identified four different flow regimes for laminar flow around a circular cylinder attached by small rods at Reynolds number of 200. They also analyzed the mechanism of fluid forces reduction by multiple small rods.

Only a small number of literature have considered the flow structures around a circular cylinder attached by multiple small rods.

Furthermore, most of these studies are carried out at high Reynolds numbers [11, 12]. Harimi et al. [13] investigated the fluid flow past a circular cylinder with three control rods arranged in equilateral triangular geometries at Re=200. The purpose of the current work is to analyze the influence of using six rods arranged in equilateral triangular geometries on the wake structures and fluid forces of the main cylinder. Also, the determination of the optimum location of small cylinders for decreasing force coefficients is another objective of this work. In addition, in order to evaluate the heat transfer rate, the Nusselt numbers for the primary cylinder and small rods are obtained and analyzed with regard to the flow profiles.

2. Governing equations and geometry

For this work, the dimensionless model equations in 2D, laminar, and unsteady mode can be expressed as below:

$$\nabla U = 0 \qquad (1)$$

$$\frac{\partial U}{\partial t} + U.\nabla U = -\nabla P + \frac{1}{\mathrm{Re}}\nabla^2 U \qquad (2)$$

$$\frac{\partial \theta}{\partial t} + U.\nabla \theta = \frac{1}{\mathrm{Re}.\mathrm{Pr}}\nabla^2 \theta \qquad (3)$$

The above equations are made dimensionless by the following parameters:

$$x = \frac{x^*}{D},\ y = \frac{y^*}{D},\ u = \frac{U_x}{U_\infty},\ v = \frac{U_y}{U_\infty},$$
$$P = \frac{P^*}{\rho U_\infty^2},\ \theta = \frac{T - T_\infty}{T_w - T_\infty},\ t = \frac{U_\infty t^*}{D} \qquad (4)$$

The boundary conditions and geometries studied shown in Fig. 1. A 40D × 24D rectangular region is applied to the model domain, and a primary cylinder with diameter of D (signed with C) is placed at the center of the domain. As indicated in Fig. 1, six small cylinders with a diameter of d (signed with R) arranged in equilateral triangular geometries surrounding the primary cylinder. The diameter ratio (d/D) and gap ratio (G/D) can determine the position of the small rods (G is the distance between two surfaces of the rod to primary cylinder). In this study, the effect of different incidence angles of α on the force coefficients is investigated. The angle interval of β for six rods surrounding the primary cylinder is 100 degrees. Also, the angle interval of γ can be defined as the angle between two small rods closer together; here it is chosen as 20 degrees. In order to avoid disturbance of the exit flow and its effects on the model predictions, the length of the downstream zone is considered very long in the model predictions.

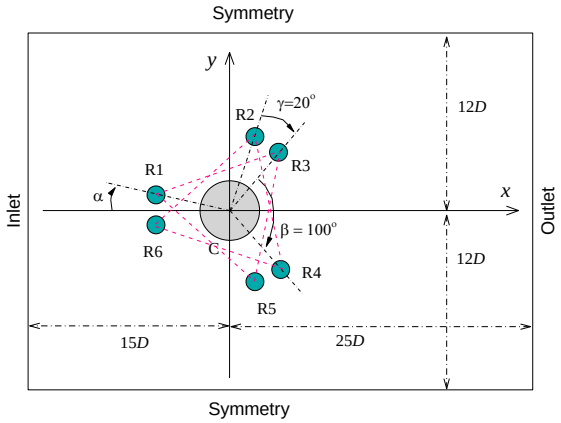

Fig. 1. Boundary conditions used and geometry for a primary cylinder attached by six small cylinders.

The boundary conditions of interest for this study are as follows:

(1) For major simulation grid:
For the inlet: u=1, v=0, and θ=0.
For the bottom and top: u=1, v=0, and θ=0.
For the outlet: $\frac{\partial \varphi}{\partial t} + U_\infty \frac{\partial \varphi}{\partial x} = 0$
where φ denotes the variables of u, v, and θ

(2) For minor simulation grid:
In the cylinder surface: u=0, v=0, and T_w=const.

Furthermore, at the beginning of the solution process (t=0), uniform incoming flow is prescribed as follows:

u=1, v=0, and θ=0.

For this study, the coefficients corresponding to drag and lift are defined by Eqs. (5) and (6), respectively. In these equations, F_D and F_L show drag and lift forces.

$$C_D = \frac{2F_D}{\rho u_\infty^2 D} = C_{DP} + C_{DF} \quad (5)$$

$$C_L = \frac{2F_L}{\rho u_\infty^2 D} = C_{LP} + C_{LF} \quad (6)$$

The Strouhal number (St) is obtained according to Eq. (7), where f is equal to the frequency of vortex shedding.

$$St = \frac{f.D}{u_\infty}, \quad (7)$$

Eqs. (8) and (9) denote the local (Nu_L) and mean Nusselt numbers (Nu), respectively:

$$Nu_L = \frac{h_L.D}{k}, \quad (8)$$

$$Nu = \frac{1}{2\pi}\int_0^{2\pi} Nu_L dL \quad (9)$$

3. Overset grid generation and solution methodology

The overset grid method is a powerful technique with flexibility in generating the grid which provides the feasibility to solve the flow around multiple geometries [14, 15]. In this approach, two separate structured grids (major and minor grid) are applied simultaneously to discretize the flow field around the cylinders. The major grid, which is a Cartesian background mesh, covers the entire computational domain while the minor grid of body, fitted around the primary cylinder and rods, is generated in regions with high temperature, pressure, and velocity gradients, and is placed on the background mesh. The governing equations are solved separately on each grid, and boundary information between the grids must be exchanged and transmitted by a suitable method. For this purpose, the nodes that called fringe points are specified in each grid to obtain data from other grids based on an interpolation algorithm.

In this numerical study, a second order accurate Crank-Nicolson scheme for discretizing the time variations and a QUICK discretization scheme for solving the convective fluxes are used. The pressure–velocity coupling is based on the Rhie-Chow algorithm [16].

4. Numerical verifications

4.1. Grid independence test

The grid independence of the results is verified using the solution in three various different grid sizes and two-time step sizes for Re=100, Pr=0.7, and 7.0. Table 1 shows the effect of grid size and time step on C_D^M, C_L^A, St, and Nu for the flow past an isolated cylinder. It can be seen from these results that no significant change is observed among the fine grid (case 1) and two the coarser grids (case 2 and case 3), as for instance, the maximum change in mean Nusselt numbers among these grids in the same time step of 0.01 is found to be around 0.27%. However, for the medium grid (H-grid size of 310 × 210 and O-grid size of 120 × 90) with increasing time steps from 0.01 to 0.02, these negligible changes are slightly increased. In general, according to Tables 1 and 2, the results show a good agreement with the other literature for all cases. By investigating the solution time, it appears that the case 2 is preferred with respect to the other cases and is, therefore, chosen for this study.

Also, values of the force coefficients, Strouhal number and mean Nusselt numbers at two Re=100 and 200 are tabulated in Table 2. By comparing the simulated results with those of other studies, the accuracy of the model is validated.

4.2. Flow past a primary cylinder attached by an upstream rod

Here, a uniform flow past two cylinders with various sizes is simulated to further validate the numerical model against the numerical results presented by [3]. The computations are performed for the range of gap ratio from 0.4 to 4.0, the diameter ratio of 0.5, and Reynolds number of 150.

Table 1. Effect of grid size and time step on C_D^M, C_L^A, St and Nu for an isolated cylinder at Re=100.

Case	H-grid size	O-grid size	Δt	C_D^M	C_L^A	St	Nu_1 (Pr=0.7)	Nu_2 (Pr=7.0)
1	370×270	190×150	0.01	1.343	0.301	0.164	5.075	11.73
2	310×210	120×90	0.01	1.344	0.307	0.165	5.061	11.73
3	260×155	90×70	0.01	1.341	0.300	0.163	5.061	11.75
4	310×210	120×90	0.02	1.341	0.296	0.166	5.055	11.57

Table 2. Comparison of the various parameters governing the problem for a single cylinder at Re =100 and 200.

	Re=100					**Re=200**				
Reference	C_D^M	C_L^A	St	Nu_1 (Pr=0.7)	Nu_2 (Pr=7.0)	C_D^M	C_L^A	St	Nu_1 (Pr=0.7)	Nu_2 (Pr=7.0)
Present study	1.344	0.307	0.165	5.075	11.73	1.338	0.664	0.194	-	-
Braza et al. [17]	1.34	0.25	0.160	-	-	1.35	0.75	0.200	-	-
Williamson* [18]	-	-	0.164	-	-	-	-	0.196	-	-
Churchill and Bernstein [19]	-	-	-	5.156	11.820	1.25	-	0.196	7.188	16.642
Hilpert and Forsch* [20]	-	-	-	5.158	11.171	-	-	-	7.162	15.431
He et al. [21]	1.35	-	0.167	-	-	1.36	-	0.198	-	-
Lu et al. [10]	1.35	0.34	0.165	-	-	1.34	0.69	0.196	-	-

*Experimental

The changes in the mean drag and root mean square RMS lift coefficients of the primary cylinder versus gap ratio are plotted in Fig. 2. As can be observed from Fig. 2(a) in the range of $0.4 \leq G/D \leq 2.0$, the drag coefficients gradually decrease as the gap ratio increase, and reach their minimum at the gap ratio of *G/D*=2.0. By further increasing the gap ratio from 2.0 to 2.5, it is observed that the drag coefficient increases suddenly, while for *G/D* > 2.5 the drag coefficients slightly increase with an increase in the gap ratio. However, despite these increases, the drag coefficients do not reach that of an isolated cylinder (i.e. 1.32). It is believed that the change in the separation point position of the downstream primary cylinder effects decreasing drag coefficients.

The overall trend of change of the drag and lift coefficients with the gap ratio is similar in $0.4 \leq G/D \leq 2.5$, while for *G/D* > 2.5 the lift coefficients show a slight decrease with increasing the gap ratio. Similarly, the sudden jump of the lift coefficient also appeares at the gap ratio of *G/D*=2.5, but unlike the drag coefficient, it gets above the value of an isolated cylinder (i.e. 0.35). Obviously, the lift fluctuations of the primary cylinder are caused by the alternative vortex shedding from it. In general, it can be found from the figures that the results obtained show a good agreement with those presented by [3].

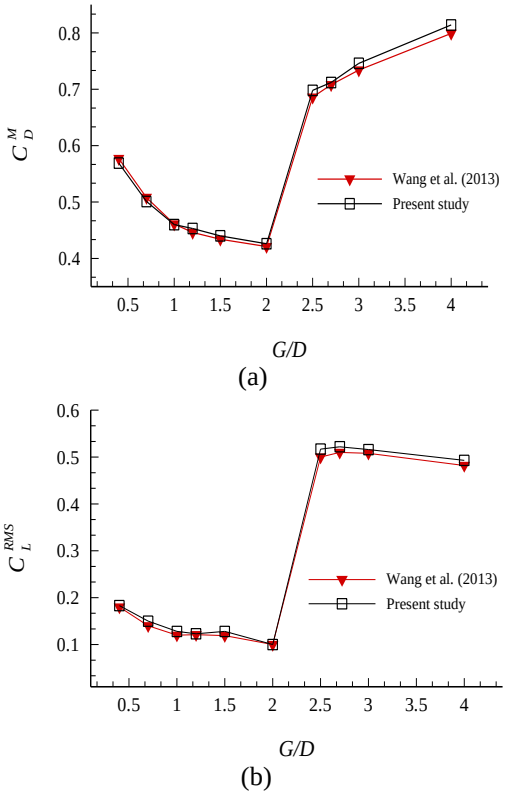

Fig. 2. Changes of force coefficients of primary cylinder with the gap ratio at Re=150 and d/D=0.5; (a) mean drag coefficients and (b) RMS values of lift coefficients.

5. Results and discussion

In this section, firstly, in order to achieve the optimum location and more efficiency of the control rods placed in desired arrangements around a primary cylinder, the influences of the flow incidence angle and gap ratio on the force coefficients, vortex characteristics, and wake structures are investigated. Then the influence of the Reynolds number as a driving parameter on the flow stability and the force coefficients of the primary cylinder is tested. The isotherm profiles, the Nusselt numbers are also studied to recognize the thermal structure around the cylinder group under consideration.

5.1. Effect of flow incidence angle on force coefficients

Fig. 3 indicates the average drag and RMS lift coefficients of the primary cylinder with six control rods versus the gap ratio *G/D* for 3 attach angles of α=0°, 10°, and 30° at Re=200 and *d/D*=0.24. It is clear that the force coefficients depend on the angle of attaching and the gap ratio. Compared with an isolated cylinder, the mean drag coefficients of the main cylinder significantly decrease for each of three angles of attaching considered. Exceptions are observed for α=0° at small gap ratio of 0.3 and also for α=10° and 30° at large gap ratios. In these cases, the drag coefficients are only slightly smaller than that of an isolated cylinder (about 20% reduction). While for example at α=0° and gap ratio of 1.3, the drag coefficient shows a decrease of about 50%. Alam et al. [7] also reported a significant reduction in the drag coefficient for a single cylinder with tripping rods at α=30° (67% reduction). However, by changing the attach angle from α=30° to α=60°, the drag coefficient is increased dramatically, which csn be attributed to the alternation of the flow structures from a subcritical flow into a natural transition flow or into a critical flow. The minimum drag force occurs at α=10° and *G/D*=0.3 (Fig. 3(a)), nevertheless the overall trend of the changes of the drag coefficients at this angle is incremental with respect to increasing the gap ratio (unlike the other two attach angles).

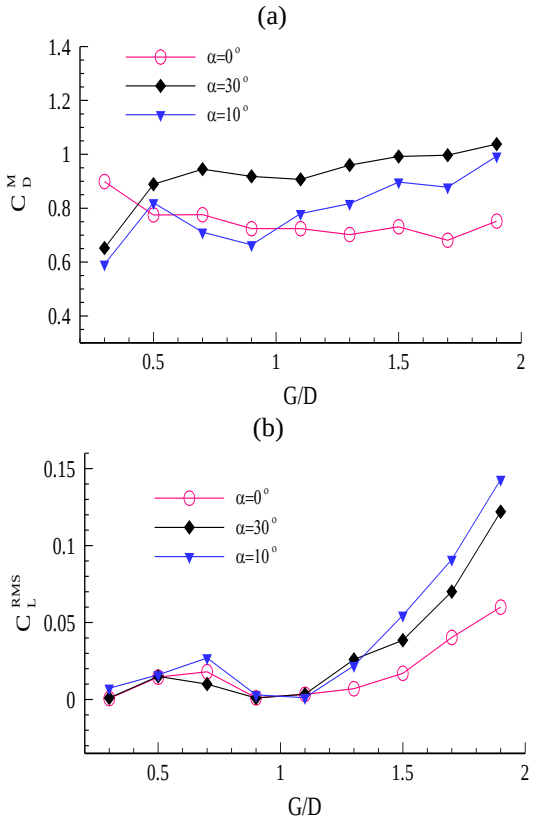

Fig. 3. Changes of drag and lift coefficients versus gap ratio *G/D* for the primary cylinder with six rods at α=0°, 10°, and 30°, *d/D*=0.24 and Re=200; (a) mean drag coefficients and (b) RMS lift coefficients.

Similarly, the lift coefficients of the primary cylinder also decrease relative to that of an isolated cylinder (i.e., 0.46) (see Fig. 3 (b)). As for small values of gap ratio at three angles of attaching considered, the lift coefficients are very near to zero or zero. For α=10° and 30°, the lift coefficients strictly increase by increasing the gap ratio, as the maximum lift force appears at *G/D*=1.9. In general, with regard to the values of the drag and lift coefficients obtained at various gap ratios, it seems that the control rods placed at α=0° have higher efficiency in suppressing the force coefficients of the primary cylinder. These results confirm well those of Wu et al. [11] and Zhu et al. [12] denoting that the multiple small cylinders are able to reduce not only the drag coefficients but also lift coefficients. But such a good agreement is not obtained with those of Zhao et al. [22].

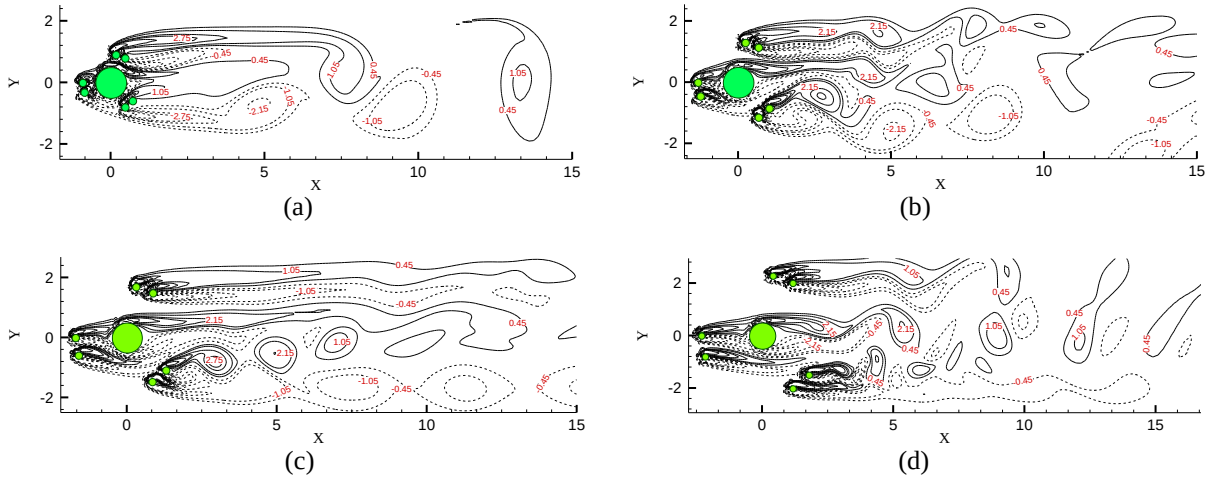

Fig. 4. Contours of vorticity around the cylinder group for various gap ratios at α=0° and Re=200; (a) *G/D*=0.3, (b) *G/D*=0.7, (c) *G/D*=1.1, and (d) *G/D*=1.7.

They reported that the lift coefficients are larger than that of a single cylinder at small values of *G/D* for an isolated cylinder with a small cylinder, and these coefficients decrease only for larger values of G/D.

5.2. Characteristics of flow patterns and wake structures

Fig. 4 plots the contours of instantaneous vorticity around the cylinders for various gap ratios at α=0°, Re=200, and the dimensionless time of t=300. As observed, for small gap ratio of 0.3, although the vortices shed alternatively in the wake downstream of the cylinders, the vortex structure in the near wake region is suppressed, and therefore the lift coefficient considerably decreases. The pressure contours and the streamlines around a single cylinder and the cylinder with rods are shown in Fig. 5. Relative to a single cylinder, the stagnation pressure on the upstream of the primary cylinder is decreased that can be attributed to the existence of the control rods (R_1 and R_6). Alam et al. [7] also found that for the cylinder with tripping rods the values of the mean pressure coefficient and the fluctuating pressure coefficient on the whole surface of the cylinder are drastically lower than that of a single cylinder, resulting in suppressing the Karman vortex street for these angles.

At G/D=0.7 (Fig. 4(b)), the interaction among the vortices shed from the control rods (R_4 and R_5) and the wake flows behind the other cylinders (i.e., C, R_1 and R_6, R_2 and R_3) leads to the scattering and instability of the vortices shed in the far wake. With further increase in the gap ratio to 1.1 (Fig. 4(c)), it is observed that the negative vortices shed from the small rods of R_4 and R_5 generate the lower row of the vortex street.

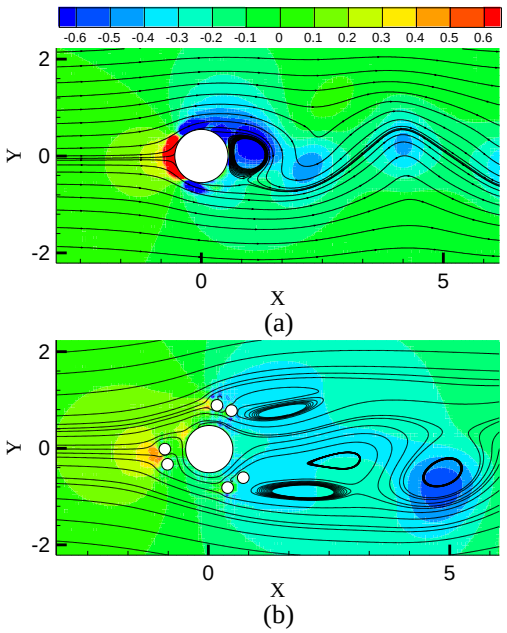

Fig. 5. Pressure distribution and streamlines at Re=200 (a) an isolated cylinder. (b) Cylinder group at α=0°, *G/D*=0.3.

However, the positive vortices generated from these rods are weak and almost disappeared. It should be noted that in this case, the vortex shedding from the cylinders is significantly suppressed (except for the rods R_4 and R_5), and only the slight instabilities are observed downstream of these cylinders. For G/D=1.7 (Fig. 4(d)), three shedding processes are observed that the interaction among those results in the formation of diagonal vortices. Thus, the wake structure gets more unstable as compared with G/D=1.1 and the lift coefficient increases.

5.3. Effect of Reynolds numbers on force coefficients

Fig. 6 shows the changes of force coefficients of the primary cylinder versus gap ratio for Re=100, 200, and 300, and the angle of attaching α=0°. As observed, the changes of the drag coefficients versus the gap ratio for all the three Reynolds numbers considered is nearly similar, although these coefficients decrease regularly with increasing Reynolds number. Indeed, the small rods placed at appropriate arrangements can be effective in suppressing the fluid forces of the primary cylinder at a wide range of Reynolds number as also reported by Zhu et al. [12]. Obviously, the reduction of drag force can be explained by the viscous effects of the shear layers around the cylinder group which by increasing the Reynolds number are weakened. Furthermore, it can be seen that for Re=200, the drag coefficients obtained for the primary cylinder are lower than those of reported by Lu et al. [10], particularly for large values of G/D.

The lift coefficients of the primary cylinder for various Re mostly remain near to zero or zero, and only with increasing Reynolds numbers at the higher gap ratios slightly enhance. Also, it is found from Fig. 6(b) that the lift coefficients for Re=200 are mostly smaller than those presented by Lu et al. [10]. Exceptions are observed at low gap ratios (i.e., G/D=0.5 and 0.7), that the lift coefficients are slightly larger than ones ones (those reported by Lu et al.). Moreover, the comparisons for other Reynolds numbers (i.e., Re=100 and 300) reveal that the drag and lift coefficients obtained in this study for most gap ratios considered are smaller than those of Lu et al. [10] (not shown here). In general, these demonstrate that the control rods placed in equilateral triangular arrangements at α=0° can be more efficient in suppressing the fluid forces acting on the primary cylinder, as compared with the arrangement applied in the study of Lu et al. [10].

Fig. 7 shows the phase diagrams for various gap ratios at Re=200 and α=0°. It is found that for the gap ratios of G/D=0.3, 0.7, 0.9, 1.1, 1.7 and 1.9, a single orbit is observed which equivalent to the periodic behavior of the flow, while for other gap ratios including G/D=0.5, 1.3 and 1.5, the flow periodicity is seriously broken and the irregular orbits appear. This phenomenon is also observed by Sarkar et al. [23], in which the orbits did not follow any particular trajectory, and the flow field entered in the regime of chaos.

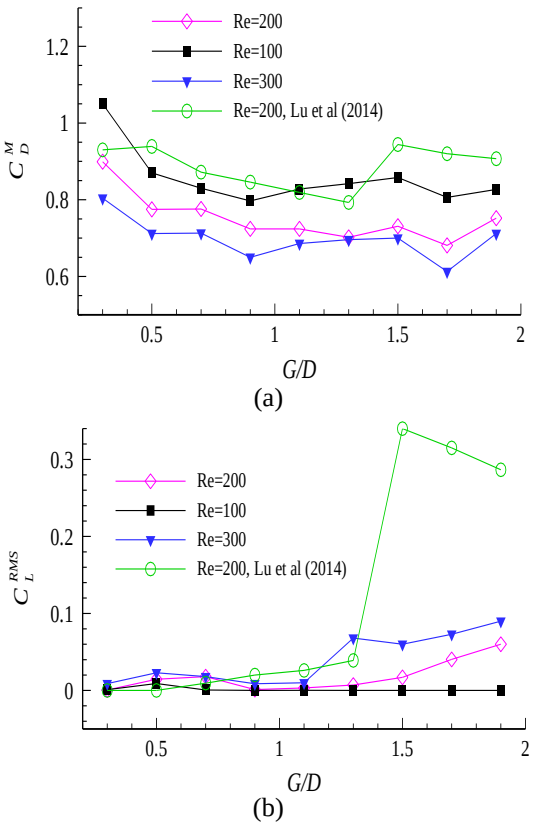

Fig. 6. Changes of drag and lift coefficients with gap ratio G/D for various Reynolds numbers at α=0°; (a) mean drag coefficient and (b) RMS lift coefficient.

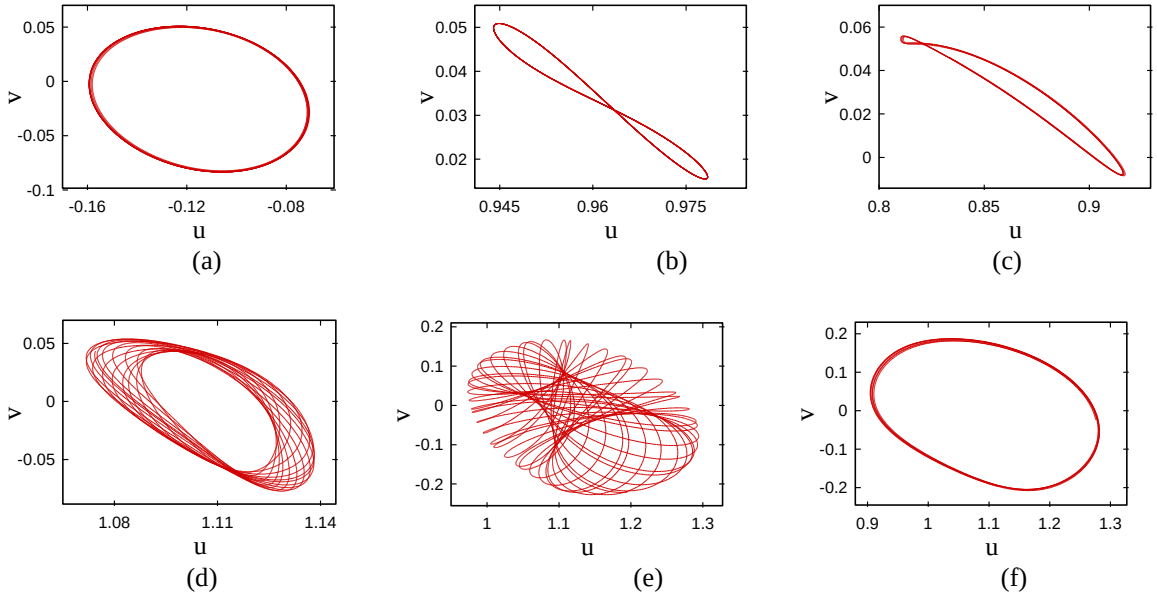

Fig. 7. Phase diagrams for various gap ratios at α=0° and Re=200; (a) *G/D*=0.3, (b) *G/D*=0.9, (c) *G/D*=1.1, (d) *G/D*=1.3, (e) *G/D*=1.5, and (f) *G/D*=1.9.

5.4. Isotherm pattern and Nusselt number

In this section, the streamlines and isotherm contours around cylinders as well as the mean and local Nu for various gap ratios at Re=200, α=0° and Pr=0.7 and 7.0 are presented. It should be noted that the heat transfer by natural convection is neglected and the physical properties of the fluid are considered to be unchanged.

Fig. 8 shows the instantaneous isotherm patterns for 3 gap ratios of *G/D*=0.3, 0.7 and 1.7. Obviously, by enhancing the Prandtl number from 0.7 to *7*.0, due to the reduction of thermal diffusion, the congestion of the isotherm contours increases as a result of the thinning of thermal boundary layer, and hence higher heat transfer rate is achieved. Similarly, as the Reynolds number is increased from Re= 100 to 300, at constant values of Prandtl number, the thermal contours start narrowing down (Not shown in Fig). Also, the isotherm contours are concentrated more in the upper region of the primary cylinder, because of the asymmetrical arrangement of the small rods with respect to the flow direction, and are seemingly more intensified for smaller gap ratio values. Clearly, the heat transfer rate increases in such regions with the high gradient, and there will be strong convection (refer to Fig. 9 (regions 36°< φ < 54°)). On the contrary, in the below region of the primary cylinder, the thermal boundary layers are less dense indicating poor temperature gradients and the lower values of the Nusselt numbers.

Generally, at the small gap ratios, the region of the low velocity and high temperature, generated between the primary cylinder and the rods, can lead to the reduction of heat transfer rate from the primary cylinder. It is notable from Fig. 8 (*G/D*=0.3 and also *G/D*=0.5) that the primary cylinder is placed in the thermal wake of two upstream rods and is most affected by high-temperature thermal boundary layers of the upstream rods. In fact, for these gap ratio values, high-temperature thermal boundary layers are merged together (primary cylinder and rods of R_1, R_4, R_5, and R_6); subsequently, the concentration of isotherms becomes weak along the downstream. Furthermore, the formation of the stagnant vortex between the primary cylinder and rod at smaller gap ratios increases the effect of the thermal wake of the rod on the primary cylinder. Although, the vortex shedding process at the small values of G/D can be found responsible for higher heat transfer rate of the primary cylinder (refer to Table 3, *G/D*=0.3 and 0.5).

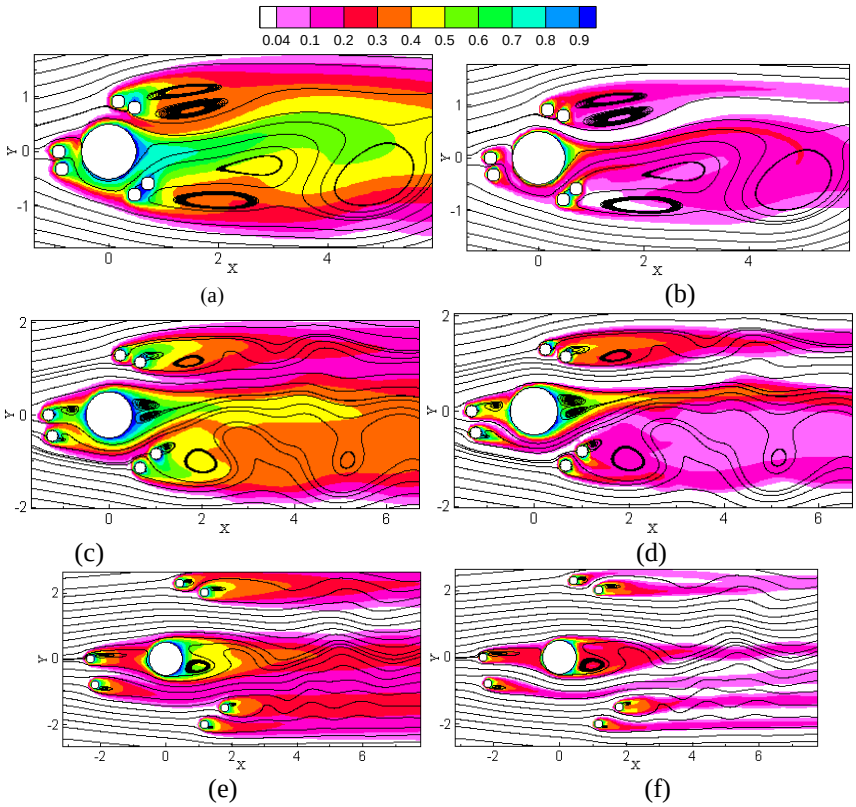

Fig. 8. The streamlines and isotherm contours around the cylinder group at Re=200 and α=0°; (a) *G/D*=0.3 and Pr=0.7, (b) *G/D*=0.3 and Pr=7.0, (c) *G/D*=0.7 and Pr=0.7, (d) *G/D*=0.7 and Pr=7.0, (e) *G/D*=1.7 and Pr=0.7, and (f) *G/D*=1.7 and Pr=7.0.

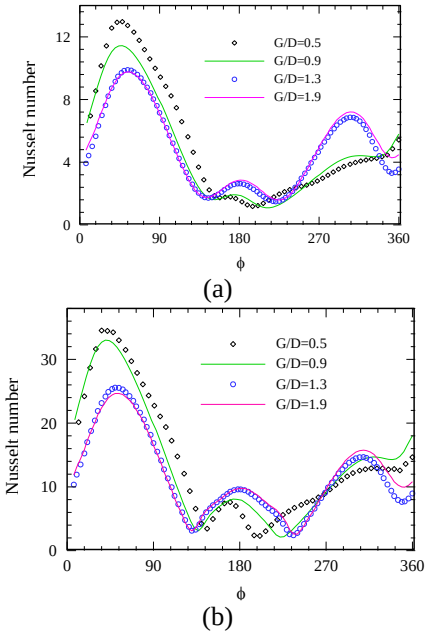

Fig. 9. The Nusselt number distributions on the primary cylinder at various gap ratios, Re=200 and α=0°; (a) Pr=0.7 and (b) Pr=7.0.

With increase of the gap ratio, effect of the thermal layers of the surrounding rods on the primary cylinder gets less and the higher heat transfer rate is expected. Also, the side rods, especially rods of R_2 and R_3 are more influenced from the straight path of flow and are less exposed to the thermal boundary layers of upstream cylinders, indicating the higher value of the Nusselt number.

The change of Nu distribution over the surface of the primary cylinder for Re=200 and Pr=0.7 and 7.0 is represented in Fig. 9. As shown, for various gap ratios, the highest value of the Nusselt number on the primary cylinder surface is observed in the zones 36°< φ < 54°, where the thickness of the boundary layer is the lowest (see the isotherm contours in Fig. 8). Evidently, the asymmetric distribution of Nusselt number along the primary cylinder surface can be attributed to the thermal wake developing of the upstream rods (R1 and R6) below the primary

cylinder. For Pr=7.0, the local Nusselt number distribution over the lower surface of the cylinder is observed not to be significant by the gap ratio. This can be attributed to the fact that in this region by the increase in gap ratio approximately no change in the thickness of the thermal boundary layer is found, and the effect of the thermal wake of the surrounding rods is also negligible.

Table 3 presents the mean Nusselt number for the primary cylinder and upstream rod (R_1) at different gap ratios and Re=200. From Table 3, the dependence of Nusselt numbers on the Prandtl number and also the gap ratio is evident. It is revealed that the mean Nusselt numbers obtained for the primary cylinder are significantly smaller than that of a single cylinder (see Table 2). With the exception of small values of gap ratios and also Pr=7.0 of the primary cylinder, it can be said that the overall trend of variation of the Nusselt numbers with the gap ratio for the primary cylinder and upstream rod of R_1 is incremental.

Table 3. The mean Nusselt number for the primary cylinder and upstream rod R1 at α=0°and Re=200.

G/D	Pr=0.7		Pr=7.0	
	Nu_C	Nu_{R1}	Nu_C	Nu_{R1}
0.3	5.126	3.009	14.857	7.464
0.5	5.203	3.167	14.022	7.029
0.7	4.139	3.188	9.528	6.947
0.9	4.746	3.260	13.668	7.159
1.1	4.739	3.310	12.197	7.253
1.3	4.738	3.339	11.560	7.408
1.5	4.899	3.346	12.173	7.470
1.7	4.908	3.342	12.067	7.474
1.9	4.929	3.409	11.904	7.569

6. Conclusions

The fluid flow past an isolated cylinder attached by six small rods arranged in equilateral triangular geometries is investigated numerically at Re=200. Based on the results obtained, a wide range of gap ratios is efficient at α=0°, as in these distances the decrease in the fluid forces on the primary cylinder is clearly evident. Moreover, in comparison with the previous studies, it seems small rods placed in equilateral triangular configurations have higher efficiency in suppressing the vortex shedding behind the primary cylinder. The investigation of the phase diagrams indicates that the flow periodicity and creating the irregular orbits for the gap ratios of *G/D*=0.5, 1.3 and 1.5 are lost. This work also indicates the results of forced convection heat transfer for the cylinders at Re=200 and Pr=0.7 and 7.0. For different gap ratios, the decrease in the heat transfer rate from the surface of the cylinders is evident and relative to that of a single cylinder. Also unexpectedly, the maximum mean of Nusselt numbers is obtained for small values of the gap ratios, that the vortex shedding process can be a response for it.

References

[1] C. Bartoli, S. Faggiani and D.Rossi,"Forced and mixed convection heat transfer from an array of cylinders to a liquid submerged jet",*Revue Generale de Thermique*, Vol. 37, No. 6, pp. 431-439,(1998).

[2] N. Mahir and Z. Altac, "Numerical investigation of convective heat transfer in unsteady flow past two cylinders in tandem arrangements", *International Journal of Heat and Fluid Flow*, Vol. 29, No. 5, pp. 1309-1318, (2008).

[3] Y. T. Wang, Z. M. Yan and H. M. Wang, "Numerical simulation of low-Reynolds number flows past two tandem cylinders of different diameters",*Water Science and Engineering*, Vol. 6, No. 4, pp. 433-445, (2013).

[4] C. H. Kim, "*The hydrodynamic interaction between two cylindrical bodies floating in beam seas. Stevens Institute of Technology*",Report SIT-OE-72-10, Stevens Institute of Technology, Hoboken, New Jersey, (1972).

[5] T. Igarashi, "Drag reduction of a square prism by flow control using a small rod", *Journal of Wind Engineering and Industrial Aerodynamics*, Vol. 69-71, pp. 141-153, (1997).

[6] C. Dalton, Y. Xu and J. C. Owen, "The suppression of lift on a circular cylinder due to vortex shedding at moderate Reynolds numbers", *Journal of Fluids*

and Structures, Vol. 15, No. 3, pp. 617-628, (2001).

[7] M. M. Alam, H. Sakamoto and M. Moriya, "Reduction of fluid forces acting on a single circular cylinder and two circular cylinders by using tripping rods", *Journal of Fluids and Structures*, Vol. 18, No. 3-4, pp. 347-366, (2003).

[8] Z. Huang, J. A. Olson, R. J. Kerekes and S. I. Green, "Numerical simulation of the flow around rows of cylinders",*Computers & Fluids*,Vol. 35, No. 5, pp. 485-491,(2006).

[9] B. S. Carmo, S. J. Sherwin, P. W. Bearman and R. H. J. Willden, "Flow-induced vibration of a circular cylinder subjected to wake interference at low Reynolds number", *Journal of Fluids and Structures*, Vol. 27, No. 4, pp. 503-522, (2011).

[10] L. Lu, M. M. Liu, B. Teng, Z. D. Cui, G. Q. Tang, M. Zhao and L. Cheng, "Numerical investigation of fluid flow past circular cylinder with multiple control rods", *Journal of Fluids and Structures*, Vol. 48, pp. 235-259 (2014).

[11] H. Wu, D. P. Sun, L. Lu, B. Teng, G. Q. Tang and J. N. Song, "Experimental investigation on the suppression of vortex-induced vibration of long flexible riser by multiple control rods", *Journal of Fluids and Structures*, Vol. 30, No. pp. 115-132, (2012).

[12] H. Zhu and J. Yao, "Numerical evaluation of passive control of VIV by small control rods", *Applied Ocean Research*, Vol. 51, pp. 93-116, (2015).

[13] S. Harimi, A. Marjani, and S. Moradi, "Numerical simulation of fluid flow and forced convection heat transfer around a circular cylinder with control rods located in equilateral triangular arrangement", *Journal of mechanical science and technology*, Vol. 30, No. 90, pp. 4239-4246 (2016).

[14] H. S. Tang, S. C. Jones and F. Sotiropoulos, "An overset-grid method for 3D unsteady incompressible flows", *Journal of Computational Physics*, Vol. 191, No. 2 pp. 567-600, (2003).

[15] J. Cai, H. M. Tsai and F. Liu, "Numerical simulation of vertical flows in the near field of jets from notched circular nozzles", *Computers & Fluids*, Vol. 39, No. 3, pp. 539-552 (2010).

[16] C. M. Rhie and W. L. Chow, "Numerical study of the turbulent flow past an airfoil with trailing edge separation", *AIAA Journal*, Vol. 21, No. 11, pp. 1525-1532, (1983).

[17] M. Braza, P. Chassaing, and H. HaMinh, "Numerical study and physical analysis of the pressure and velocity fields in the near wake of a circular cylinder", *Journal of Fluid Mechanics*, Vol. 165, pp. 79-130, (1986).

[18] C. H. K. Williamson, "2-D and3-D aspects of the wake of a cylinder and their relation to wake computations", *American Mathematical Society, Lectures in Applied Mathematics* (1991).

[19] S. W. Churchill, M. J. Bernstein, "A correlating equation for forced convection from gases and liquids to a circular cylinder in cross flow", *Journal of Heat Transfer*, Vol. 99, No. 2, pp. 300-306 (1977).

[20] R. Hilpert, Geb. Forsch, *Ingenieurwes*, Vol. 4, pp. 215 (1933).

[21] J. W. He, R. Glowinski, R. Metcalfe, A. Nordlander, and J. Periaux, "Active control and drag optimization for flow past a circular cylinder I: oscillatory cylinder rotation", *Journal of Compuational Physics*, Vol. 163, No. 1, pp. 83-117 (2000).

[22] M. Zhao, L. Cheng, B. Teng and D. F. Liang, "Numerical simulation of viscous flow past two circular cylinders of different diameters", *Applied Ocean Research*, Vol. 27, No. 1, pp. 39-55 (2005).

[23] S. Sarkar, A. Dalal and G. Biswas, "Mixed convective heat transfer from two identical square cylinders in cross flow at Re =100", *International Journal of Heat and Mass Transfer*,Vol. 53, No. 13-14, pp. 2628-2642 (2010).

How to cite this paper:

S. Harimi and Azam Marjani, "Numerical investigation on the effects of six control rods arranged in equilateral triangular configurations on the fluid flow and forced convection heat transfer from a circular cylinder" *Journal of Computational and Applied Research in Mechanical Engineering*, Vol. 9, No. 1, pp. 31-43, (2019).

DOI: 10.22061/jcarme.2019.2716.1274

URL: http://jcarme.sru.ac.ir/?_action=showPDF&article=1035